

## Factors contributing to plastic strain amplification in slip dominated deformation of magnesium alloys

This content has been downloaded from IOPscience. Please scroll down to see the full text.

2015 Modelling Simul. Mater. Sci. Eng. 23 085002

(<http://iopscience.iop.org/0965-0393/23/8/085002>)

View [the table of contents for this issue](#), or go to the [journal homepage](#) for more

Download details:

IP Address: 192.12.184.7

This content was downloaded on 05/10/2015 at 15:34

Please note that [terms and conditions apply](#).

# Factors contributing to plastic strain amplification in slip dominated deformation of magnesium alloys

C W Sinclair<sup>1</sup>, G Martin<sup>2,3</sup> and R A Lebensohn<sup>4</sup>

<sup>1</sup> Department of Materials Engineering, The University of British Columbia, 309-6350 Stores Road, Vancouver, Canada

<sup>2</sup> Université de Grenoble Alpes, SIMAP, F-38000 Grenoble, France

<sup>3</sup> CNRS, SIMAP, F-38000 Grenoble, France

<sup>4</sup> Materials Science and Technology Division, Los Alamos National Laboratory, Los Alamos, NM 87544, USA

E-mail: [chad.sinclair@ubc.ca](mailto:chad.sinclair@ubc.ca)

Received 7 March 2015, revised 2 July 2015

Accepted for publication 22 July 2015

Published 5 October 2015



## Abstract

While plastic strains are never distributed uniformly in polycrystals, it has recently been shown experimentally that the distribution can be extremely heterogeneous in magnesium polycrystals even when the deformation is dominated by slip. Here, we attempt to provide insight into the (macroscopic) factors that contribute to this strain amplification and to explain, from a local perspective, the origins of this strain amplification. To do this, full field VPFFT crystal plasticity simulations have been performed under the simplifying assumption that twinning is inoperative. It is shown that the experimentally observed heterogeneity can be reproduced when a sufficiently high anisotropy in slip system strength is assumed. This can be further accentuated by a weakening of the texture.

Keywords: plasticity, crystal plasticity, modelling, magnesium, heterogeneity

(Some figures may appear in colour only in the online journal)

## 1. Introduction

While hexagonal closed packed (hcp) crystals generally satisfy the Von Mises criterion of having more than five independent deformation modes [1], the fact that not all modes are equally easy to operate poses a challenge for compatible polycrystalline deformation. Only under specific conditions are the available ‘soft’ mechanisms sufficient to accommodate an imposed deformation. Thus, it is often required to operate one or more ‘hard’ systems. This

results in a macroscopic response that is highly anisotropic, with certain orientations of single crystals being significantly ‘softer’ than others (see e.g. [2]). In the case of a polycrystal, the situation becomes more complex as satisfying compatibility and equilibrium between neighbouring crystals of different orientation may require local deformation fields far from those imposed macroscopically, e.g. [3–9]. In this case it may be preferable for the material to select spatially inhomogeneous solutions to accommodate the macroscopic boundary conditions. Such inhomogeneity may be manifested within individual grains as deformation twins or at a more mesoscopic scale as shear bands [3–5, 9, 10]. Even when the imposed deformation and (average) crystal orientation of polycrystals are selected to promote slip rather than twinning, plasticity organizes in a spatially non-uniform fashion. Such behaviour has been shown in Ti [11, 12], hexagonal ice [13–15] and Mg polycrystals [7–9] where plastic strain amplification occurs close to some, but not all, grain boundaries. While similar to the plastic strain (and stress) amplification found near grain boundaries in cubic materials (e.g. Cu [16]), the heightened anisotropy of hcp polycrystals leads to as much as 4 times the level of strain amplification compared to cubic polycrystals [8].

In a recent experimental study [8], the plastic strain distribution measured via microscale digital image correlation on the surface of a ZEK-100 magnesium sheet alloy was reported. Under deformation conditions leading to slip dominated deformation (i.e. tensile deformation parallel to the rolling direction of the sheet) it was shown that the plastic strain distributed inhomogeneously, with some regions undergoing more than four times the macroscopically imposed plastic strain. Correspondingly, other regions were found to undergo nearly zero plastic strain. This inhomogeneous distribution of plastic strain was found to be stable, meaning that the distribution of plastic strain remained self similar with increasing imposed tensile strain. Using a full-field FFT based micro-mechanical model [17] it was shown that the anisotropy of slip system strength could explain the observed behaviour. In particular, it was shown that assigning an initial critical resolved shear stress for prism and/or pyramidal slip that is  $>8$  times that of basal slip could reproduce both the macroscopic tensile stress-strain response as well as the DIC measured local distribution of plastic strain. What wasn’t explored, however, was the origins of this strain amplification at some locations within the microstructure but not at others.

In this work we have attempted to quantify the most important factors affecting the magnitude and location of strain amplification in hcp Mg polycrystals deforming by slip. To do this, full field visco-plastic FFT crystal plasticity simulations have been performed on synthetic microstructures designed so as to reproduce basic features of the ZEK-100 Mg alloy previously studied experimentally [8]. This work starts by examining the effect of slip system level anisotropy, texture strength, and magnitude of plastic strain on the micro-scale plastic strain distribution. From this, the local conditions that explain strain amplification at certain grain boundaries are identified.

## II. Methodology

Following on the previous work of Martin *et al* [8], the crystal plasticity simulations reported here have made use of the full-field spectral VPFFT model [15, 17, 18]. This technique predicts the local strain-rate field by means of iteratively solving the equations of equilibrium and compatibility for a periodic polycrystal. This requires an iterative calculation of convolutions between the Green’s function and a polarization field determined from the heterogeneity of the material [17]. When Fourier transformed these convolutions become multiplications making the computation of the solution of the governing equations very efficient [19, 20].

Using the same procedure as described previously by Martin *et al* [8], the synthetic microstructure input into the VPFFT simulations was constructed starting from a polycrystal containing 752 grains generated from phase-field grain growth simulations (see [8, 21] for details). This microstructure was discretized onto a mesh of  $64 \times 64 \times 64$  Fourier points, each point being defined by its position and crystallographic orientation. The same crystallographic orientation was assigned to each Fourier point in a single grain, the crystallographic orientations being either assigned based on experimentally measured bulk texture, or based on a synthetic texture as will be described below.

Uniaxial tensile tests were simulated by imposing a macroscopic tensile strain-rate parallel to the RD direction and assuming isotropic, isochoric contraction in the transverse directions. While magnesium polycrystals are known to be plastically anisotropic, the fact that the texture in the ND-TD plane is relatively weak (see figure 1) means that macroscopically the contraction in the ND and TD directions is very similar. All shear stresses were also assumed to be equal to zero. While the behaviour of the polycrystals studied here was not found to be perfectly transversely isotropic in the simulations, leading to some stresses in the transverse directions, these stresses never exceeded 10% of the tensile stress.

Locally, the constitutive relationship relating the strain rate ( $\dot{\epsilon}_{ij}(x)$ ) and the deviatoric stress ( $\sigma'(\mathbf{x})$ ) was taken as the classic rate-dependent expression,

$$\dot{\epsilon}_{ij}(\mathbf{x}) = \sum_{s=1}^{N_s} m_{ij}^s(\mathbf{x}) \dot{\gamma}^s(\mathbf{x}) \quad (1)$$

where the strain rate on a given slip system is,

$$\dot{\gamma}^s(\mathbf{x}) = \dot{\gamma}_0 \left( \frac{\mathbf{m}^s(\mathbf{x}) : \sigma'(\mathbf{x})}{\tau_c^s(\mathbf{x})} \right)^n \text{sgn}(\mathbf{m}^s(\mathbf{x}) : \sigma'(\mathbf{x})) \quad (2)$$

Here,  $N_s$  is the number of slip systems,  $m^s(\mathbf{x})$  is the symmetric Schmid tensor, and  $\tau_c^s$  is the critical resolved shear stress for slip system  $s$  (see e.g. [23] for further details).

Basal, prismatic, pyramidal  $\langle a \rangle$  and pyramidal  $\langle c + a \rangle$  slip systems were considered in these simulations, the critical resolved shear stress for all slip systems being assumed to harden according to a Voce-type hardening law,

$$\tau_c^s = \tau_0 + \tau_1 \left[ 1 - \exp\left(-\frac{\theta_0 \Gamma_c}{\tau_1}\right) \right] \quad (3)$$

Here,  $\tau_0$  is the initial critical resolved shear stress,  $\tau_1$  is a scaling stress and  $\theta_0$  is the initial hardening rate. The total accumulated plastic shear strain in each Fourier point is denoted  $\Gamma_c$ . The initial hardening rate,  $\theta_0$ , was assumed to be 127 MPa and 170 MPa (between  $\mu/100$  and  $\mu/300$ ,  $\mu$  being the shear modulus) for basal slip and non-basal slip respectively, as previously argued in references [8, 22]. Consistent with literature (see, e.g. [22, 24–27]) we take basal slip to have the lowest value of  $\tau_c$ . Twinning is not considered in these simulations consistent with the experimental observation [8] that twinning does not play a significant role (up to the onset of necking) for the textures and alloys of interest here. One further simplifying assumption made here is that all non-basal slip systems share the same parameters  $\tau_0$  and  $\tau_1$ . It was shown previously that the results of importance from these simulations do not change if the hardening parameters for prism and pyramidal slip are differentiated [8].

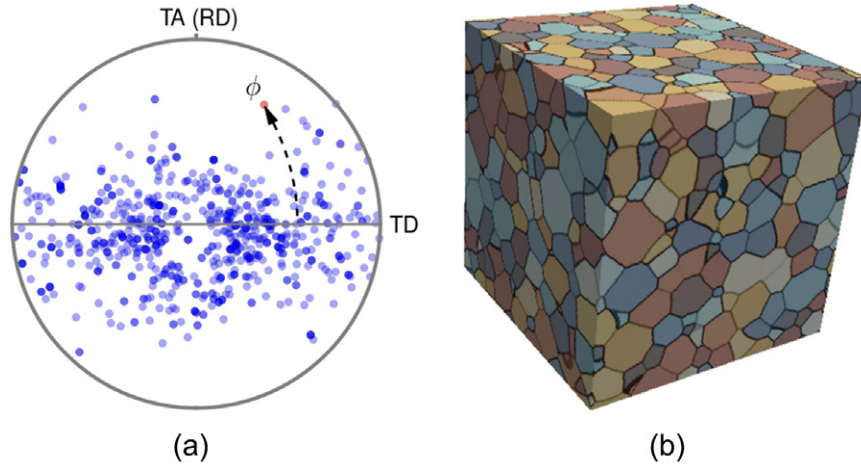


**Figure 1.** (a) Discrete  $\{0001\}$  pole figure for texture used in simulations on the effect of slip system strength anisotropy (varying  $M$ ). This texture was constructed by statistically sampling the texture experimentally measured from a ZEK-100 alloy sheet [8]. Also shown is the definition of the angle  $|\phi|$  which is used here to denote the angular distance of the  $c$ -axis of a given grain (here the red grain) with respect to the plane perpendicular to the tensile axis (TA). All pole figures in this paper have been plotted using the same convention as used here. (b) Synthetic microstructure used in all simulations, each grain being coloured randomly.

### III. Effect of slip system anisotropy on plastic strain distribution

While previous work [8] reported that  $M = \tau_0^{\text{non-basal}}/\tau_0^{\text{basal}} > 8$  was required to reproduce both the experimentally measured stress–strain response and local (grain scale) distribution of plastic strain in tension, the quantitative relationship between the microscale distribution of plastic strain and  $M$  has not been described.

To study this relationship systematically, the synthetic microstructure shown in figure 1 was constructed as described above. Each Fourier point in a grain was assigned the same crystallographic orientation, these orientations taken from the experimentally measured texture of a ZEK-100 alloy [8]. The probability of selecting a given orientation for a grain was weighted based on the volume fraction of that orientation ( $\pm 5^\circ$ ) in the experimental texture. This texture is weak compared to other Mg alloys, though it still shows a preferred alignment of  $\langle 0001 \rangle$  ( $c$ -axis) towards the normal direction (ND) of the sheet. In this case, however, a significant spread towards the transverse direction (TD) of the sheet (figure 1) is observed. The majority of grains have their  $\langle 0001 \rangle$  within  $20^\circ$  of the plane containing the ND and TD directions, i.e. with  $c$ -axes  $70\text{--}90^\circ$  from the tensile axis. In the following analysis we will often make use of the absolute value of the angle  $|\phi|$ , defined as the angle between a given grain's  $\langle 0001 \rangle$  and the ND-TD plane (figure 1).

With this texture, if slip were assumed to occur with the same CRSS and hardening on all (basal and non-basal) slip systems, one would expect that grains with  $|\phi| \approx 0^\circ$  would deform predominantly by prism and pyramidal slip, since the Schmid factor for basal slip would be close to zero. With increasing  $|\phi|$  towards  $45^\circ$  the fraction of basal slip would increase towards 1. Based on similar logic, increasing  $M$  would be expected to increase the stress required to initiate (and continue) yielding in grains with  $|\phi|$  close to zero, while those grains with  $|\phi| > 20^\circ$ , where slip is already dominated by basal systems, would be expected to remain

**Table 1.** Slip system level Voce hardening law parameters used in simulations.

	$M = 2$		$M = 4$		$M = 8$		$M = 14$		$M = 20$	
	$\tau_0$	$\tau_1$								
Basal	48	15	27	15	15	15	10	15	7	15
Non-Basal	96	75	108	45	120	45	140	15	140	15

Note: All values in units of MPa.

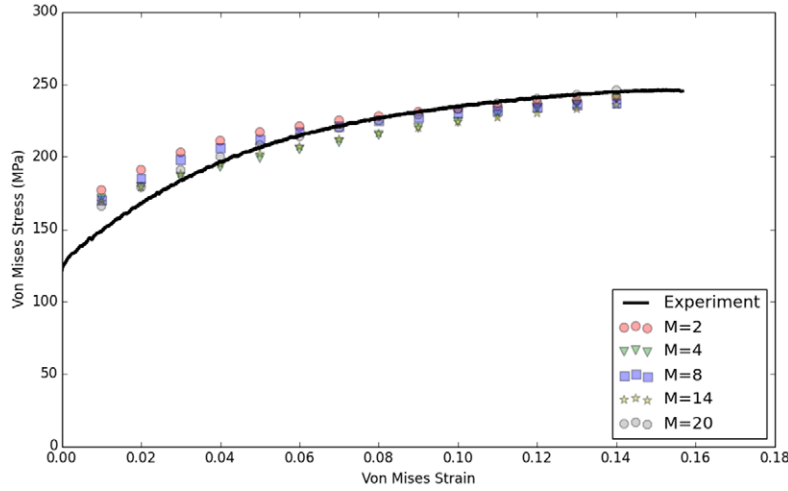


**Figure 2.** Experimental stress–strain curve for a ZEK-100 sheet specimen [8] alongside the predicted stress–strain response for VPFFT simulations with  $M = 2, 4, 8, 14$  and 20.

easy to deform. The material is required, in this case, to find a solution to maintain equilibrium and compatibility between neighbouring grains now having increasing levels of mechanical contrast.

To test how the material accommodates this increasing level of grain to grain anisotropy, VPFFT simulations were performed for different values of  $M$  (see table 1). For each value of  $M$ , the remaining hardening parameters ( $\tau_0^{\text{basal}}, \tau_1^{\text{basal}}, \tau_1^{\text{non-basal}}$ ) were adjusted so as to give a similar prediction of the macroscopic stress–strain response (figure 2).

While the parameters for each value of  $M$  predict the macroscopic stress–strain response with nearly equal precision, how the stresses and strains are partitioned through the microstructure changes significantly. Figure 3 shows two-dimensional slices through the RVE where the magnitude of the Von Mises equivalent strain ( $\epsilon_{\text{vm}}$ ) are shown. Significant variation of the magnitude of plastic strain is observed, with an apparent preference for higher strains close to grain boundaries [8]. It can also be seen that changing the value of  $M$  (holding the microstructure fixed) does not change the location of local strain amplification but does significantly change the magnitude of the strain amplification. To simplify the discussion, one can eliminate the explicit consideration of the spatial variation of plastic strain magnitude by looking at the microscale strains based on the statistical distribution of their magnitudes. Figure 4 shows the probability density function for the local value of  $\epsilon_{11}$  normalized by the average (macroscopic) value of tensile strain ( $\langle \epsilon_{11} \rangle$ ), i.e. the distribution of  $\epsilon_{11}/\langle \epsilon_{11} \rangle$  measured at each Fourier point. These are shown for different levels of macroscopically imposed strain illustrating that the local strain distribution remains self-similar throughout the simulated

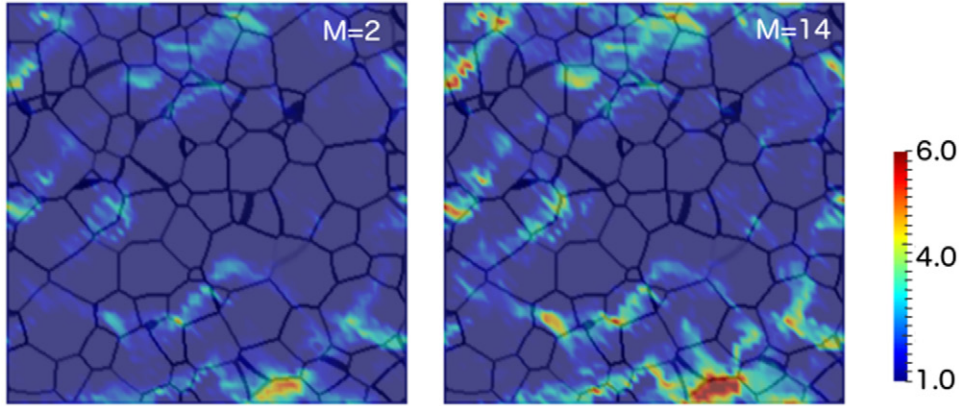


**Figure 3.** Slice through simulated microstructures at  $\epsilon_{vm} = 0.05$  where colours show magnitude of  $\epsilon_{vm}/\langle\epsilon_{vm}\rangle$  for (a)  $M = 2$  and (b)  $M = 14$ .

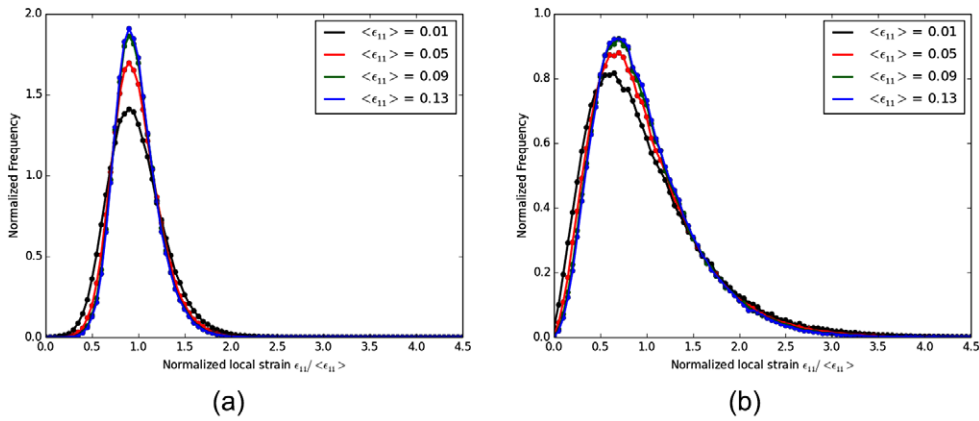


**Figure 4.** Distribution of the normalized strain  $\epsilon_{11}/\langle\epsilon_{11}\rangle$  as a function of the macroscopically imposed plastic strain,  $\langle\epsilon_{11}\rangle$  for (a)  $M = 2$  and (b)  $M = 14$ . As can be seen, the distributions become self similar after the first step of simulated deformation [8].

tensile test [8]. Thus, while some regions strain much more than others, this distribution is stable and does not undergo bifurcation (strain localization). Given this result, we will focus throughout the rest of this paper on comparing such local plastic strain distributions at a single value of  $\langle\epsilon_{11}\rangle = 0.05$ .

The systematic variation of the probability density function for the  $\epsilon_{11}/\langle\epsilon_{11}\rangle$  taken from each Fourier point (hereon referred to as the ‘local plastic strain distribution’) as a function of  $M$  is shown in figure 5. The distributions clearly widen with increasing  $M$ , in particular the high-strain tail of the distribution. The widening of the distributions with  $M$  can be captured if the width of the distributions is represented by their standard deviation, this being shown in figure 6.

As discussed above, one would expect, based on a simple Schmid analysis, that as  $M$  increases so too should the fraction of basal slip. This is clearly seen in figure 6 where the fraction basal slip for the polycrystal increases from  $\sim 0.2$  at  $M = 2$  to  $\sim 0.7$  at  $M = 20$ .

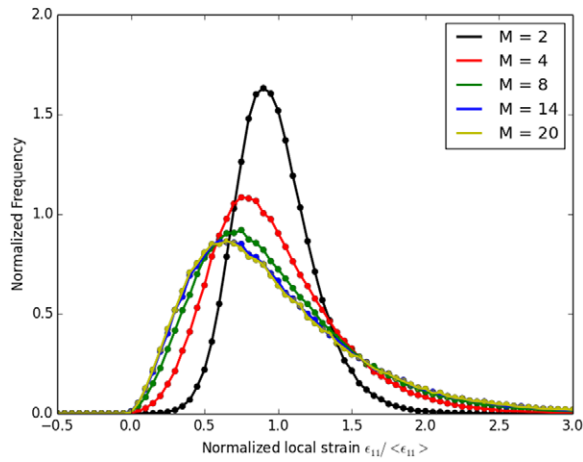


**Figure 5.** The distribution of  $\epsilon_{11}$  normalized by the macroscopic applied  $\langle \epsilon_{11} \rangle$  for  $M = 2, 4, 8, 14$  and  $20$ . Here,  $\langle \epsilon_{11} \rangle = 0.04$ .

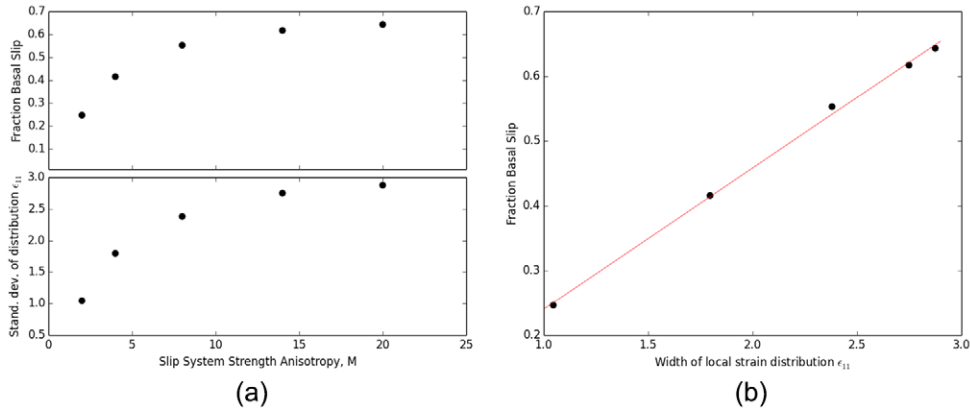


**Figure 6.** (a) Average fraction of total shear strain due to slip carried by basal slip systems and width of the local plastic strain ( $\epsilon_{11}$ ) as a function of  $M$  (b) The linear correlation between width of the plastic strain distribution ( $\epsilon_{11}$ ) and the fraction of basal slip for the different levels of slip system anisotropy tested.

Interestingly, it was found that the width of the plastic strain distribution could be correlated linearly to the fraction of basal slip for the polycrystal (figure 6). One can view this as a result of the fraction basal slip being a proxy for the increasing mechanical contrast between the various grains, the increase in basal slip indicating the degree to which grains with low  $|\phi|$  (e.g.  $\lesssim 20^\circ$ ) harden as  $M$  increases. This is consistent with the results in figure 7 where it is shown that increasing  $M$ , increases the fraction of basal slip in grains with low values of  $|\phi|$  while leaving the fraction basal slip in grains with high values of  $|\phi|$  nearly unchanged.

A natural expectation would be that for large  $M$ , those grains with low  $|\phi|$  (e.g.  $\lesssim 20^\circ$ ) would deform plastically at higher stresses than those with higher values of  $|\phi|$ . This would result in a strong variation of the magnitude of plastic strain and stress with the angle  $|\phi|$ . This would result in grains with low  $|\phi|$  being responsible for the spreading of the local plastic strain

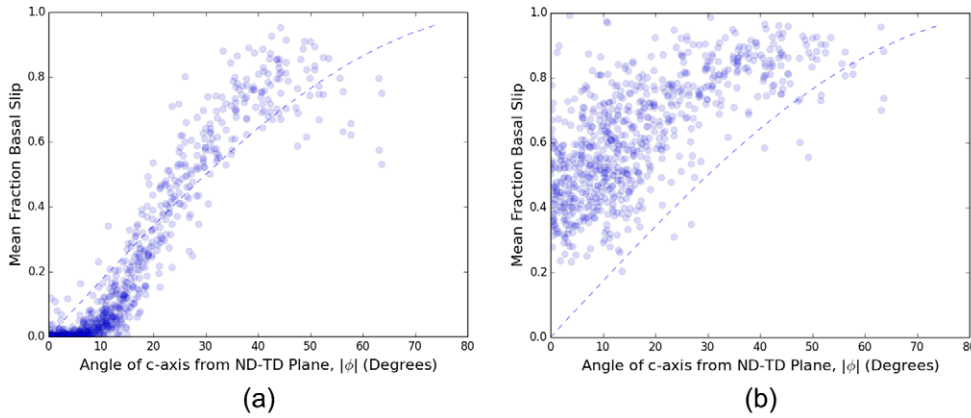


**Figure 7.** Fraction of basal slip in each grain as a function of the angle between the grain's  $c$ -axis and the ND-TD plane ( $|\phi|$ ) for (a)  $M = 2$  and (b)  $M = 14$ . The dashed line shows  $\sin(|\phi|)$  which is proportional to the Schmid factor for basal slip.

distribution to higher values of  $\epsilon_{11}/\langle\epsilon_{11}\rangle$  (figure 4). This interpretation is wrong, however, as revealed by figure 8 where it is shown that the average and maximum values of  $\epsilon_{vm}$  and  $\sigma_{vm}$  in each grain show no systematic variation with the angle  $|\phi|$ .

#### IV. Effect of bulk texture on plastic strain distribution

Increasing the grain-to-grain mechanical contrast was accomplished above by increasing  $M$ , the mechanical anisotropy at the slip system level. One can achieve nearly the same effect, however, by fixing  $M > 2$  and modifying the texture. To show this, synthetic textures were generated based on the ZEK-100 texture (figure 1) as a guide. Starting from a single grain having an orientation such that  $\langle 0001 \rangle \parallel \text{ND}$  and  $\langle 10\bar{1}0 \rangle \parallel \text{RD}$ , a random rotation angle  $-180^\circ \leq \theta \leq 180^\circ$  was selected and the orientation was rotated about RD. Next, this orientation was rotated again about the TD by an angle randomly selected between two limits  $-\alpha^\circ \leq \theta \leq \alpha^\circ$ , where  $\alpha$  was selected to limit the maximum value of  $|\phi|$  for a grain. The grain orientations developed in this way were randomly assigned to the grains in the same synthetic polycrystal shown figure 1. Figure 9 illustrates  $\{0001\}$  pole figures for three textures created in this way. Simulations were then performed in the same way as those described above except that in all cases the slip system level hardening parameters associated with  $M = 14$  in table 1 were used.

Just as increasing  $M$  increased the width of the plastic strain distribution so too does spreading the texture (figure 10). Starting from the texture where all grains have  $\langle 0001 \rangle$  within the range  $|\phi| \pm 5^\circ$  only a narrow local plastic strain distribution is obtained similar to that obtained above for  $M = 2$ . As the texture was spread, the width of the distribution (measured by its standard deviation) increased substantially, mirroring the change in width of the distribution when  $M$  was increased. Again, one can look at the fraction of basal slip for the polycrystal as a measure of the mechanical contrast between grains. At low texture spread slip is predominantly accommodated by non-basal slip but as the texture widens and grains are added with higher  $|\phi|$  the fraction basal slip increases. As in the case of varying  $M$  it was found that the fraction basal slip correlates linearly with the width of the plastic strain distribution (figure 11).

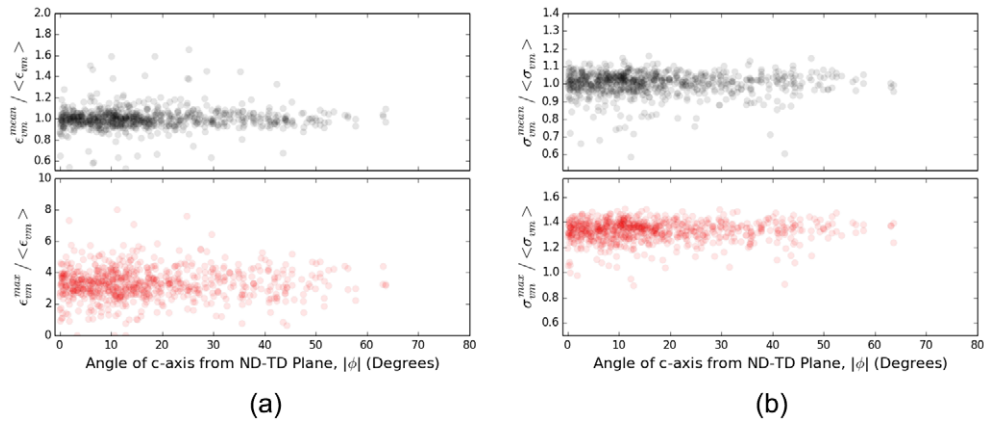


**Figure 8.** The variation of the mean and maximum value of the normalized strain (a)  $\epsilon_{vm} / \langle \epsilon_{vm} \rangle$  and (b) stress  $\sigma_{vm} / \langle \sigma_{vm} \rangle$  in each grain for  $M = 14$ .

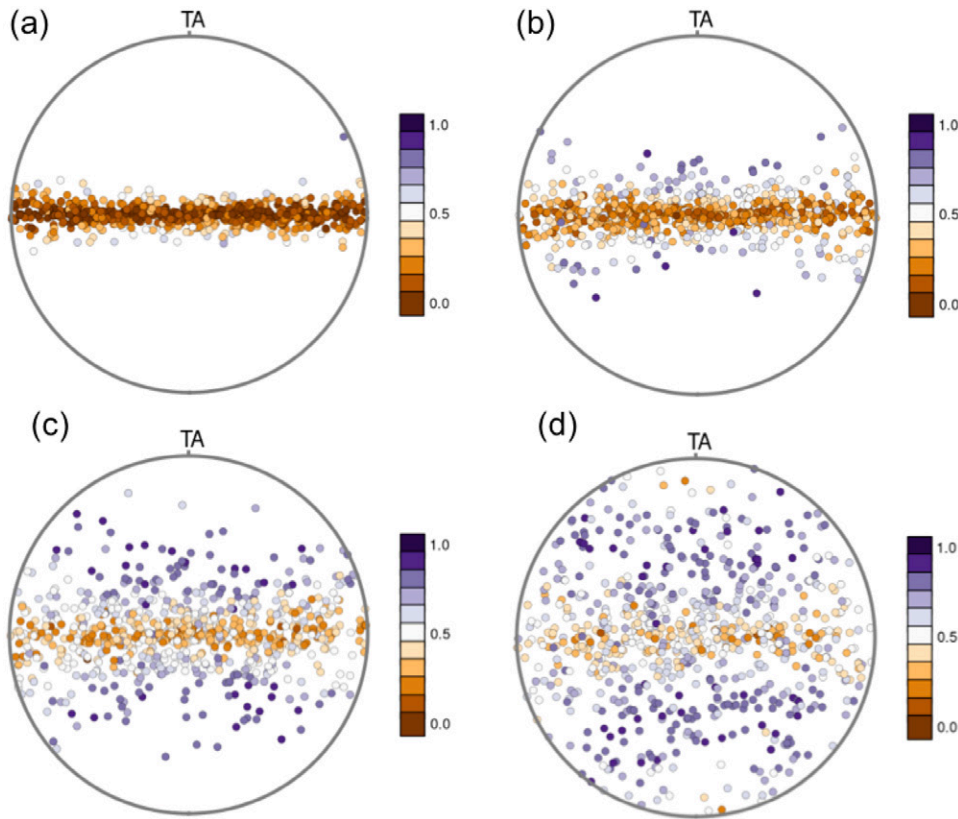


**Figure 9.** Synthetic textures were produced to evaluate the effect of the texture spread on plastic strain distribution. Here  $\{0001\}$  pole figures are shown for angular spreads of the textures of (a)  $\alpha = 5^\circ$ , (b)  $\alpha = 10^\circ$ , (c)  $\alpha = 19^\circ$  and (d)  $\alpha = 32^\circ$ . The point corresponding to the orientation of each grain is coloured according to the average fraction of basal slip in that grain at a macroscopic imposed strain of  $\langle \epsilon_{vm} \rangle = 0.05$ . The tensile direction is denoted as TA.

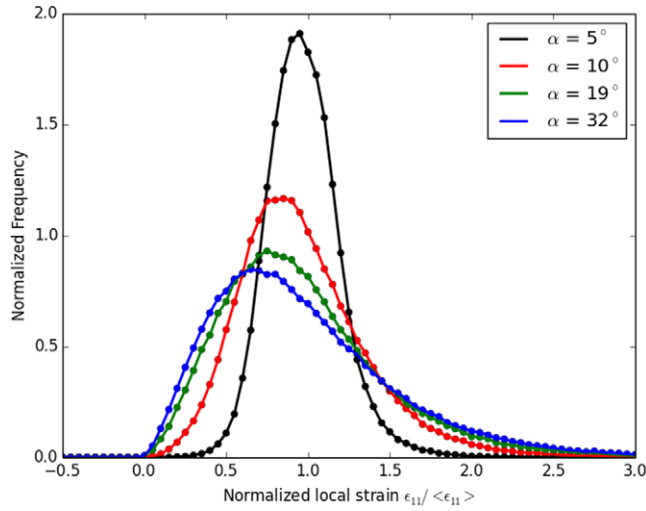


**Figure 10.** Distribution function for the local plastic strain  $\epsilon_{11}$  (component parallel to the tensile direction) for  $M = 14$  and macroscopic Von Mises strain  $\langle \epsilon_{vm} \rangle = 0.05$ . The effect of different spread of the texture ( $\alpha$ ) is shown.

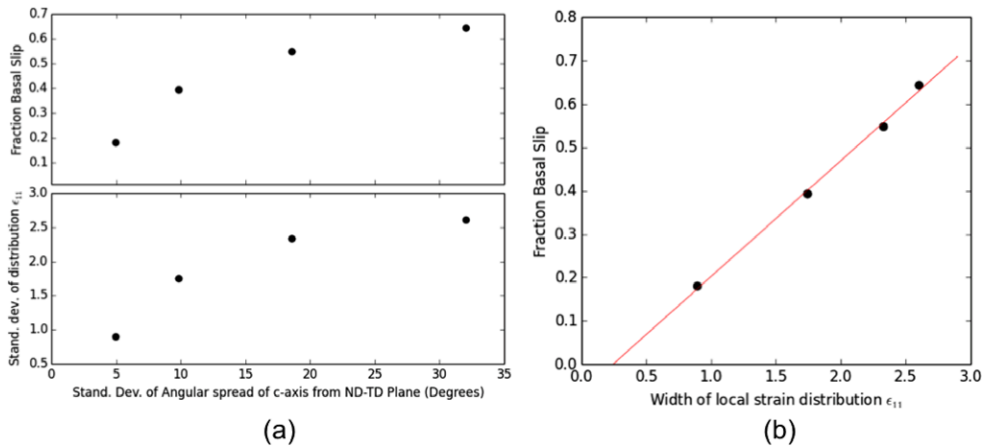


**Figure 11.** (a) The effect of broadening the texture (increasing spread of  $c$ -axis towards the tensile (RD) direction) on the fraction of basal slip and the width of the distribution of local  $\epsilon_{11}$ . (b) The linear correlation between width of the texture distribution and width of the plastic strain distribution is evident.

While one might imagine the fraction basal slip shown in figure 11 to increase with increasing texture spread simply because the new grains added to the polycrystal have higher Schmid factors for basal slip, this simplified interpretation would miss the fact that the fraction basal slip also increases for grains with low values of  $|\phi|$  (e.g. for  $|\phi| \lesssim 20^\circ$ ). Figure 12 shows that the average fraction basal slip at  $|\phi| = 0$  increases from  $\approx 0$  for  $\alpha = 5^\circ$  to  $\sim 0.3$  for  $\alpha = 19^\circ$ . This is also revealed in figure 9 where the colour of each point in the pole figure corresponds to the average fraction basal slip in each grain.

Again, one might be tempted to make that assumption that the increasing width of the plastic strain distribution with increasing  $\alpha$  arises from the addition of ‘soft’ grains well oriented

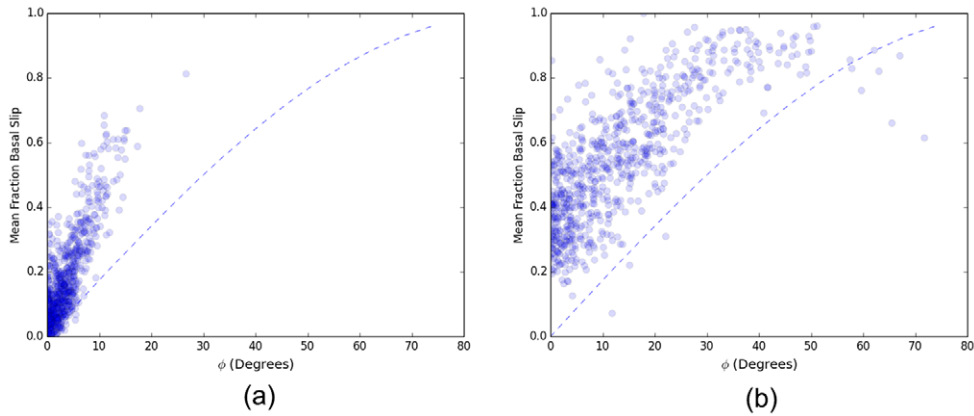


**Figure 12.** The average fraction basal slip in each grain as a function of  $|\phi|$  for (a)  $\alpha = 5^\circ$  and (b)  $\alpha = 19^\circ$ .

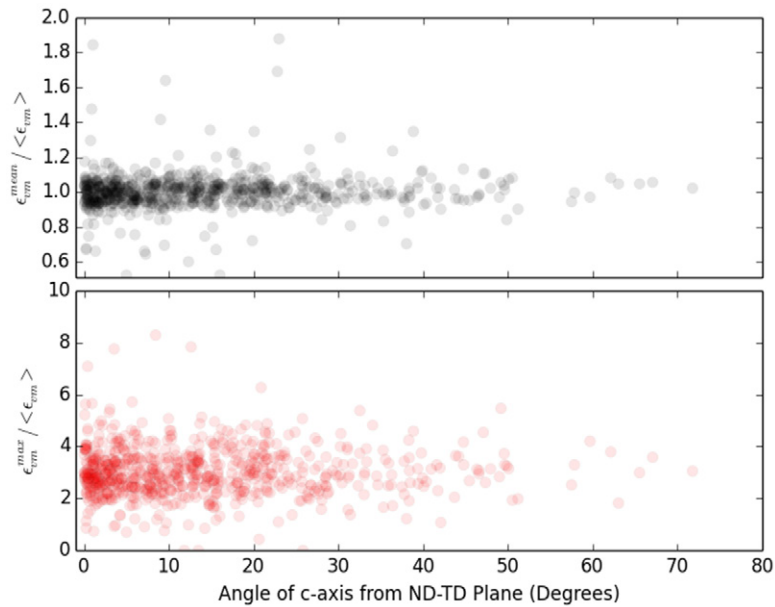


**Figure 13.** The variation of the maximum and average value of  $\epsilon_{vm}$  in each grain as a function of the angle  $|\phi|$  for  $\alpha = 19^\circ$  showing the same lack of correlation as for figure 8.

for basal slip ( $|\phi| > 20^\circ$ ), these being the grains that contribute to the high end of the local plastic strain distribution. Like figure 8, figure 13 shows that there is no clear correlation between either the maximum or average value of plastic strain in each grain and  $|\phi|$ .

## V. What conditions predict the location of regions of high strain amplification?

While the above results clearly show the effect of slip system level anisotropy and texture spread on the distribution of local strain at the microstructural scale, it is not possible from

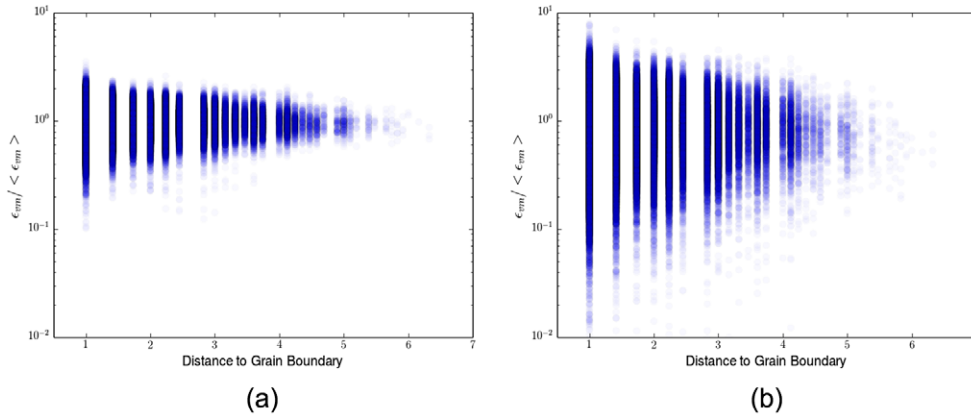


**Figure 14.** The correlation between the plastic strain ( $\epsilon_{vm}/\langle\epsilon_{vm}\rangle$ ) at a Fourier point and its distance to the nearest grain boundary for (a)  $M = 2$  and (b)  $M = 14$ .

these results alone to explain physically the origins of the width of the plastic strain distribution. In particular, one would like to understand what conditions lead to the regions of locally high plastic strain. Returning to figure 3 one can see that the regions of high plastic strain appear to locate close to grain boundaries. Indeed, one can see this statistically if the euclidean distance between each Fourier point and the nearest grain boundary is measured and this distance plotted versus the magnitude of plastic strain (figure 14) [8].

While it was argued above that there was no clear correspondence between the local magnitude of plastic strain and angle  $|\phi|$ , one might still anticipate that grains deforming predominantly by basal slip to be more likely to undergo large plastic strain. While there is generally a dependence between  $|\phi|$  and fraction slip (see figures 12 and 7) one can also see that a significant fraction of grains with low  $|\phi|$  deform predominantly by basal slip when  $M > 8$  and when the texture spread is sufficiently wide. To investigate this further we have selected to look at the case corresponding to  $M = 14$  described above. Figure 15 shows a plot of  $\epsilon_{vm}/\langle\epsilon_{vm}\rangle$  versus fraction basal slip for each Fourier point in the simulation domain. While the data is strongly scattered, particularly for  $\epsilon_{vm}/\langle\epsilon_{vm}\rangle \approx 1$ , there is a clear tendency for those Fourier points exhibiting the highest levels of plastic strain to deform predominantly by basal slip. This is seen more clearly if the Fourier points are binned based on the magnitude of plastic strain and the average value for the fraction basal slip plotted for each bin. In this case one can clearly see that the fraction basal slip is highest for those Fourier points experiencing the highest levels of strain.

It is important to note, however, that figure 15 also shows that the fraction basal slip for a given Fourier point does not provide a unique indicator of the magnitude of plastic strain. Indeed, most Fourier points with high fraction basal slip exhibit less than the average plastic strain (i.e.  $\epsilon_{vm}/\langle\epsilon_{vm}\rangle < 1$ ). Returning to figures 3 and 14, those regions exhibiting high plastic strain also appear to be close to grain boundaries, yet not all grain boundary regions deforming predominantly by basal slip exhibit high levels of plastic strain amplification.

To investigate further the conditions that lead to some grain boundary regions accruing high levels of plastic strain, the correlation between such regions and their neighbouring Fourier points across the nearest grain boundary were investigated (figure 16). To do this all Fourier points having  $\epsilon_{vm}/\langle\epsilon_{vm}\rangle > 3.5$  were identified. Next all those Fourier points located in the same grain and forming a contiguous group were identified, any groups containing less

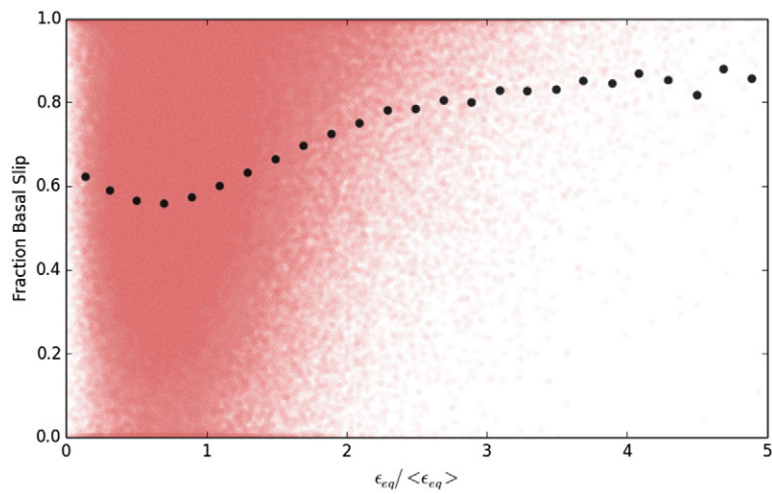


**Figure 15.** The fraction basal slip in each Fourier point as a function of the strain amplitude ( $\epsilon_{vm}/\langle\epsilon_{vm}\rangle$ ) in that Fourier point is shown as the red points. To illustrate the trends more clearly, the data was binned in terms  $\epsilon_{vm}/\langle\epsilon_{vm}\rangle$  and the average value of the fraction basal slip was calculated. This is plotted as the black points.

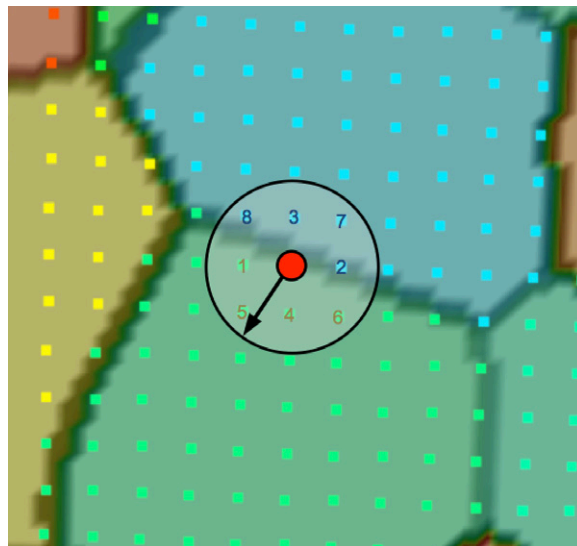


**Figure 16.** An illustration of how the neighbour search was performed starting from one Fourier point (circled red), where all Fourier points to second nearest neighbour in an adjacent grain (here points 2,3,7 and 8) are identified.

than two Fourier points were removed from further consideration. For each group, the Fourier point having the largest value of  $\epsilon_{vm}/\langle\epsilon_{vm}\rangle$  was identified and its nearest neighbour Fourier points (up to second nearest neighbour) were identified. The nearest neighbouring point(s) not located in the same grain were then selected for further analysis.

Figure 17 shows the same data as in figure 15 but overlaid are the specific Fourier points identified above, i.e. the point with highest  $\epsilon_{vm}/\langle\epsilon_{vm}\rangle$  in a group and its nearest neighbour

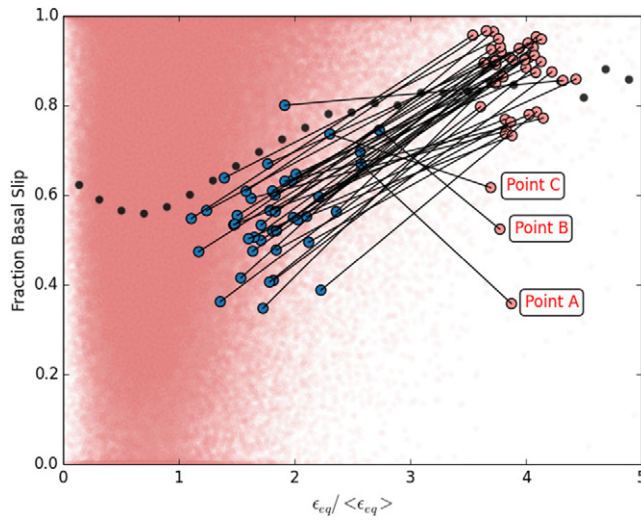


**Figure 17.** The same data as in figure 15 but superimposed are the specific Fourier points having high levels of strain amplification (red circles) and the nearest adjacent Fourier points that are in a neighbouring grain (blue circles). These points are connected by a black line to show that they are neighbours in the simulated microstructure. Three anomalous points (labeled ‘A’, ‘B’ and ‘C’) are also noted. These points have high strain but low fractions basal slip compared to their nearest neighbours.

across a grain boundary. The red circles show the local strain and fraction basal slip for the points having high plastic strain, while the blue points show the corresponding neighbour Fourier points across the nearest grain boundary. The black lines connect neighbouring pairs of points across the grain boundary. One can clearly see that while the neighbouring points across the grain boundary all accrue less plastic strain than the high strain regions, in all but three cases they do so at higher than the mean fraction basal slip. Thus, those near grain boundary regions undergoing the largest strain amplification appear to arise from grains well oriented for basal slip being adjacent to grains deforming by a mix of basal and non-basal slip.

One can look at the same data set in terms of the local stresses. Figure 18 shows a plot of fraction basal slip as a function of Von Mises stress intensity for each Fourier point in the simulation as well as the binned and average values, this having been done in the same way as for the plastic strain in figure 17. Also plotted here, like in figure 17, are the neighbouring Fourier points corresponding to high strain amplification and the Fourier point from the neighbouring grain. Looking at this data we see that the distribution in stress is much lower than the distribution in plastic strain, with  $\|\sigma_{vm}/\langle\sigma_{vm}\rangle\|_{max}$  being  $\leq 1.4$ . The regions of high strain amplification are seen to generally correspond to Fourier points deforming at lower stress than the adjacent Fourier points in the neighbouring grain. Interestingly, nearly all of these Fourier point pairs deform under stresses that are at or below the average stress  $\sigma_{vm}/\langle\sigma_{vm}\rangle \leq 1$ .

The conclusion of this analysis would therefore be that most of the regions of highest strain amplification arise at grain boundaries separating a grain deforming predominantly by (‘soft’) basal slip and a grain deforming with a much higher proportion of ‘hard’ non-basal slip. Predicting which grains (or combinations of grains) will exhibit such behaviour based on orientation alone (i.e. without performing a full field simulation), however, is impossible as it appears that the local neighbour–neighbour interactions strongly affect the local state of stress, the active slip systems and plastic strain. This is clearly exhibited by the three outlier

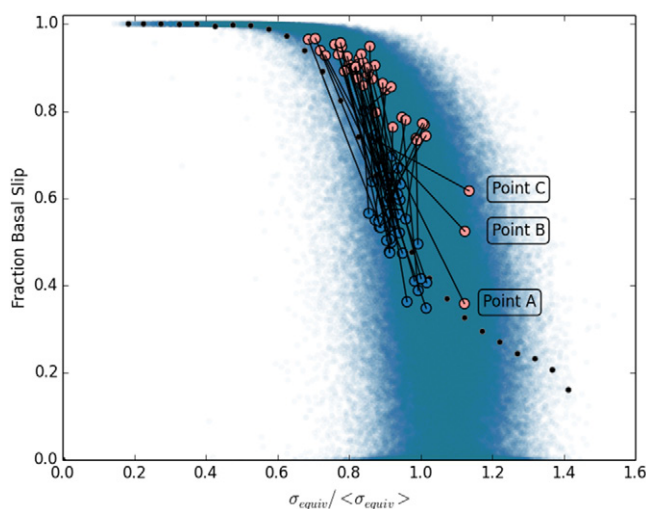


**Figure 18.** The Fourier point by Fourier point stress amplification  $\sigma_{vm}/\langle\sigma_{vm}\rangle$  plotted as a function of the fraction basal slip along with the specific points corresponding to specific Fourier points having high levels of strain amplification (red circles) and the nearest adjacent Fourier points that are in a neighbouring grain (blue circles). These points are connected by a black line to show that they are neighbours in the simulated microstructure. The same anomalous points (labeled ‘A’, ‘B’ and ‘C’) as in figure 17 are also noted.

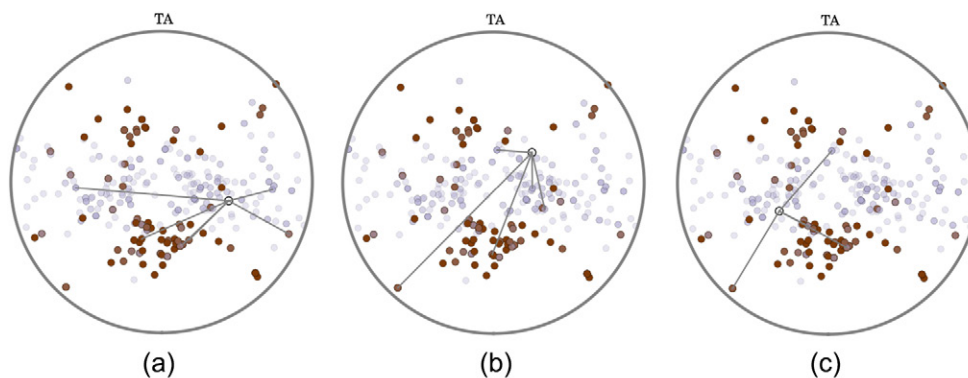


**Figure 19.** {0001} pole figures showing the orientation of the regions (before deformation) that undergo high strain amplification (red) and their neighbouring grains (grey). In particular, three anomalous regions, i.e. those that undergo large strain amplification but with low fraction basal slip identified as Points A, B and C in figures 17 and 18, are highlighted here. They are shown in white, the straight lines connecting these orientations to the orientations of their neighbouring grains. (a) Grains neighbouring Point A (b) Grains neighbouring Point B and (c) Grains neighbouring Point C.

regions in figures 17 and 18. Figure 17 shows three regions where the Fourier point exhibiting the highest level of strain amplification has a *lower* fraction basal slip than the adjacent Fourier point across the grain boundary. These points also appear as outliers in figure 18 as they are the three red points that exhibit a higher value of  $\sigma_{vm}/\langle\sigma_{vm}\rangle$  than the adjacent Fourier

points across the grain boundary. Notably these points also are seen to deform at stresses significantly higher than  $\langle\sigma_{vm}\rangle$ .

Some clue to the anomalous behaviour of these three regions can be seen if one looks more broadly at their neighbourhood. Figure 19 shows a  $\{0001\}$  pole figure where the orientation of each Fourier point corresponding to the red points in figures 17 and 18 are shown as red points. Plotted as light grey points are the orientations of all of the grains that neighbour the grain containing the region of high strain amplification. Each of these pole figures highlights one of the three high-strain Fourier points, showing (by means of lines) which of the grains it neighbours. One can notice that these three points of high strain amplification appear to have relatively low  $|\phi|$ , this generally accounting for their lower than average fraction basal slip. Also important, however, is the observation that they are all surrounded by grains that themselves have high plastic strain amplification. The average plastic strain in the grains neighbouring these three anomalous points have an average value of  $\epsilon_{vm}/\langle\epsilon_{vm}\rangle = 1.6$  compared to a value of  $\epsilon_{vm}/\langle\epsilon_{vm}\rangle = 1.3$  for the neighbours to all of the other high strain amplification points. This would suggest that these anomalous regions undergo high local plastic strain owing to longer range correlations; the fact that the grains in the immediate vicinity undergo larger than average levels of plastic strain, forcing a region that would otherwise not experience large plastic strain amplification to maintain compatibility and equilibrium by deforming to larger strains.

Finally, it is worth reflecting on the fact that the simulations performed here do not explicitly consider the properties of the grain boundaries themselves. There have been a number of recent studies that have aimed to evaluate the importance of grain boundary orientation with respect to the ease of slip transmission, see e.g. [28, 29], in crystal plasticity simulations. Our results appear consistent with the conclusion of Bieler *et al* [28] who found in their analysis of local plastic strains that it was unnecessary to include slip transfer in crystal plasticity simulations to obtain a good statistical, spatial prediction of plastic strains in both cubic and hexagonal metals. Taking such analyses one step further to consider behaviours that are more sensitive to the intrinsic nature of the boundary, e.g. fracture nucleation or grain boundary sliding, may require the inclusion of this next level of detail in modelling.

## VI. Conclusion

Through the use of full-field crystal plasticity simulations, the local strain amplification previously measured experimentally in the slip dominated deformation of a ZEK-100 alloy [8], has been reproduced when sufficiently different values of the CRSS for basal and non-basal slip systems are assumed. The degree of plastic strain inhomogeneity was shown to also depend sensitively on texture. As the texture spreads away from the ND-TD plane more strain heterogeneity appears as the mechanical contrast between neighbouring grains grows. The observed strain amplification, occurring preferentially at grain boundaries, arises from grain-to-grain differences in the mechanical response linked to orientation. In the majority of cases it was found that strain amplification occurred on one side of a grain boundary, in a grain deforming predominantly by basal slip, adjacent to a grain deforming predominantly by non-basal slip. In this case the amplification of strain on one side of a grain occurs to accommodate a ‘harder’ adjacent region. In a small number of cases, large strain amplification was found in locations where the fraction basal slip was lower than in the adjacent grain. In this case it was argued that longer ranged correlations between the strain in a grain (or part of a grain) and the strain accommodated by its neighbouring grains leads to this apparently anomalous behaviour.

## Acknowledgments

The authors wish to express their gratitude to NSERC-Canada for the financial support of this work through the MagNET Strategic Research Network.

## References

- [1] Tegart W J McG 1964 *Phil. Mag.* **9** 339
- [2] Sánchez-Martin R, Pérez-Prado M T, Segurado J, Bohlen J, Gutiérrez-Urrutia I, Llorca J and Molina-Aldareguia J M 2014 *Acta Mater.* **71** 283
- [3] Sandlöbes S, Zaeferrer S, Schestakow I, Yi S and Gonzalez-Martinez R 2011 *Acta Mater.* **59** 429
- [4] Scott J, Miles M, Fullwood D, Adams B, Khosravani A and Mishra R K 2013 *Metall. Mater. Trans. A* **44** 512
- [5] Barnett M R, Nave M D and Bettles C J 2004 *Mater. Sci. Eng. A* **386** 205
- [6] Barnett M R and Stanford N 2007 *Scr. Mater.* **57** 1125
- [7] Martin G, Sinclair C W and Schmitt J-H 2013 *Scr. Mater.* **68** 695
- [8] Martin G, Sinclair C W and Lebensohn R A 2014 *Mater. Sci. Eng. A* **603** 37
- [9] Martin G, Sinclair C W, Poole W J and Azizi-Alizamini H 2015 *JOM* **67** 1761–73
- [10] Wang F, Sandlöbes S, Diehl M, Sharma L, Roters F and Raabe D 2014 *Acta Mater.* **80** 77
- [11] Bieler T R, Crimp M A, Yang Y, Wang L, Eisenlohr P, Mason D E, Liu W and Ice G E 2009 *JOM* **61** 45
- [12] Wang L, Barabash R I, Yang Y, Bieler T R, Crimp M A, Eisenlohr P, Liu W and Ice G E 2011 *Metall. Mater. Trans. A* **42** 626
- [13] Montagnat M, Blackford J R, Piazzolo S, Arnaud L and Lebensohn R A 2011 *Earth Planet. Sci. Lett.* **305** 153
- [14] Grennerat F, Montagnat M, Castelnau O, Vacher P, Moulinec H, Suquet P and Duval P 2012 *Acta Mater.* **60** 3655
- [15] Lebensohn R A, Montagnat M, Mansuy P, Duval P, Meysonnier J and Philip A 2009 *Acta Mater.* **57** 1405
- [16] Rollett A D, Lebensohn R A, Groeber M, Choi Y, Li J and Rohrer G S 2010 *Modelling Simul. Mater. Sci. Eng.* **18** 074005
- [17] Lebensohn A 2001 *Acta Mater.* **49** 2723
- [18] Lebensohn R A, Brenner R, Castelnau O and Rollett A D 2008 *Acta Mater.* **56** 3914
- [19] Prakash A and Lebensohn R A 2009 *Modelling Simul. Mater. Sci. Eng.* **17** 064010
- [20] Liu B, Raabe D, Roters F, Eisenlohr P and Lebensohn R A 2010 *Modelling Simul. Mater. Sci. Eng.* **18** 085005
- [21] Shahandeh S, Greenwood M and Miltzer M 2012 *Modelling Simul. Mater. Sci. Eng.* **20** 065008
- [22] Jain J, Poole W J and Sinclair C W 2012 *Mater. Sci. Eng. A* **547** 128
- [23] Lebensohn R A and Tomé C N 1993 *Acta Metall. Mater.* **41** 2611
- [24] Jain A and Agnew S R 2007 *Mater. Sci. Eng. A* **462** 29
- [25] Bohlen J, Nürnberg M R, Senn J W, Letzig D and Agnew S R 2007 *Acta Mater.* **55** 2101
- [26] Agnew S R and Duygulu Ö 2005 *Int. J. Plast.* **21** 1161
- [27] Agnew S R, Brown D W and Tomé C N 2006 *Acta Mater.* **54** 4841
- [28] Bieler T R, Eisenlohr P, Zhang C, Phukan H J and Crimp M A 2014 *Curr. Opin. Sol. State Mater. Sci.* **18** 212
- [29] Yang Y, Wang L, Zambaldi C, Eisenlohr P, Barabash R, Liu W, Stout M R, Crimp M A and Bieler T R 2011 *JOM* **63** 66